Pergamon

Int. J. Heat Mass Transfer. Vol. 38, No. 17, pp. 3209–3217, 1995

0017–9310/95 $9.50+0.00

0017–9310(95)00070–4

Boundary-layer control by heat and mass transfer

S. HUBBARD and N. RILEY†

School of Mathematics, University of East Anglia, Norwich NR4 7TJ, U.K.

(*Received* 4 *July* 1994 *and in final form* 20 *January* 1995)

Abstract—Slot injection into the flow over a Joukowski aerofoil is considered. A narrow slot is placed close to the leading edge and the effect of injection of fluid from this on the boundary layer over the aerofoil is examined. In particular it is shown how separation may be delayed and, when cold fluid is injected, how the surface downstream from separation may be cooled.

1. INTRODUCTION

In this paper we consider two-dimensional, laminar, incompressible, boundary-layer flow over an aerodynamic surface. Fluid may be injected from a slot into the flow. Recent work on slot injection into the flow past a solid surface includes the inviscid studies of Fitt and co-workers [1, 2]. In [1], the fluid is injected normal to the boundary and the injected layer of fluid is much thicker than any viscous boundary layers that may be present. The analysis in [2] extends that of [1] to a slot geometry which includes a drop of height from the boundary upstream to that downstream, thereby allowing oblique injection. Injection into viscous boundary layers has a long history. Much of the work reported relates to the flat-plate boundary layer with normal injection. The work of Klemp and Acrivos [3] exemplifies this. The blowing velocity is on the boundary-layer scale, $O(Re^{-1/2}U_0)$ where Re is the Reynolds number and U_0 the free-stream speed. If the variation of this is as the inverse square root from the leading edge, a similarity reduction of the boundary-layer equations is available. When blowing on this scale is large the boundary layer, thickness $O(Re^{-1/2}c)$, where c is a typical length, is blown off the plate to the relatively large distance $O(Re^{-1/3}c)$. Catherall *et al.* [4] have shown that if the blowing velocity is uniform on the boundary-layer scale then, even though small, this will lead to a singular behaviour of the solution which they interpret as flow separation. For supersonic flow Smith and Stewartson [5, 6] have extended these studies into a regime where the blowing velocity is much stronger, namely $O(Re^{-3/8}U_0)$. In particular, in [5] the injected fluid emerges from the flat plate through a slot of width $O(Re^{-3/8}c)$. These scales of blowing velocity and slot width are chosen in order that the 'triple-deck' theory may be employed. This allows for the interaction between the boundary layer and the outer inviscid flow, due to this relatively strong blowing, to be accommodated. Riley [7, 8] has extended this slot-blowing example to incompressible flow, and to cases in which the injected fluid emerges at an oblique angle to the free stream. These slot-injection studies are local, in the sense that they demonstrate how, locally, the flow over a flat plate responds to this type of injection and helps to promote flow separation. Our aim is to demonstrate that oblique injection, when the angle between the surface and injected-flow direction is small, can energize the flow and delay separation. Such injection may also be used to cool the surface over which the injected fluid flows. Earlier work on this type of film cooling has been surveyed by Goldstein [9].

Our choice of aerodynamic surface is the classical Joukowski aerofoil. This suits our requirements admirably. From the point of attachment the pressure falls rapidly to a minimum, and then rises monotonically to the trailing edge. It is not well designed, in the sense that flow separation is readily provoked; and even at modest incidence the separation point moves to the leading-edge region, immediately downstream from the suction peak. It is in this region that we locate our injection slot, in length about 5% of chord. Fluid is injected from the slot, with components normal and tangential to the surface, on the boundary-layer scale. As a consequence, although the blowing speed may be large, the mass injection rates are modest. We demonstrate that this type of injection can delay separation to the trailing edge, even when in the absence of injected fluid flow separation is close to the leading edge. Furthermore, we show that the injection of cold fluid from the slot has a significant cooling effect on the surface downstream from it. We work within a classical boundary-layer framework. However, we do analyse the boundary-layer displacement effect upon the outer flow. This shows that the fluid ahead of the slot is, as expected, accelerated. But the modification to the flow due to this effect will be negligible at high Reynolds numbers.

† Author to whom correspondence should be addressed.

NOMENCLATURE

a	circle radius in z-plane
c	aerofoil chord
J	measure of injection strength
K	circulation
l	injection slot length
p	pressure
p_0	free stream pressure
Re	Reynolds number
s	arc-length on body surface
T	temperature
T_w	wall temperature
T_∞	upstream temperature
T_0	measure of injected fluid temperature
u	streamwise boundary-layer velocity
u_e	slip velocity at aerofoil
u_J	injection profile
U_0	free-stream speed
v	crossflow boundary-layer velocity
w	complex potential
y	boundary-layer normal co-ordinate
$z' = x' + iy'$	complex variable in physical plane.

Greek symbols

α	angle of incidence
α_e	effective incidence
β	$\alpha_e - \alpha$
δ	width of slot boundary layer
ε	$Re^{-1/2}$
ζ	complex variable in transformed plane, $\xi + i\eta$
θ	polar angle in z-plane
λ	parameter in Joukowski transformation
μ	measure of aerofoil thickness
ν	kinematic viscosity
ρ	density
σ	Prandtl number
τ	wall shear stress
ϕ	$2\alpha + \beta + \pi - \theta$
χ	injection angle
ψ	measure of aerofoil camber.

Subscripts

i	index for streamwise discretization
j	index for cross-stream discretization.

Superscripts

r	iteration number in numerical process.

The plan of our paper is as follows. In Section 2 we consider the inviscid flow. This includes not only a brief description of the classical Joukowski aerofoil, but also the modification to the inviscid flow due to displacement effects. These are represented by a source distribution over the surface of the aerofoil. In Section 3 the viscous boundary-layer flow, and the simulated slot flow are described. This section also includes a discussion of the viscous displacement effect. Section 4 considers the corresponding thermal boundary layer. The numerical techniques, based on finite differences, that we have used to solve the boundary-layer equations are introduced in Section 5, with the results therefrom presented in Section 6. We note that our hierarchical approach to the calculation of the flow field, in which the leading-order inviscid flow is determined, followed by the boundary-layer calculation, is only justified when the effect of the boundary layer on the outer flow is negligible. The displacement effect associated with injection is shown to be small provided $Re \gtrsim 10^4$, and the effect of flow separation on the outer flow can only strictly be ignored when separation takes place close to the trailing edge, as at the higher injection rates. Of course, injection will result in inflectional boundary-layer profiles which are likely to be unstable at high Reynolds number and our calculations are limited to laminar flow throughout.

2. INVISCID FLOWS

2.1. *The basic inviscid flow*

As we have already indicated in Section 1, it is the boundary layer on a classical Joukowski aerofoil that we seek to influence by injection. We briefly review here the construction of the flow past such an aerofoil.

Consider the circle $z' = a e^{i\theta}$ in the $z'(= x' + iy')$ plane. The conformal transformation, where now $z' = az$,

$$\zeta = z + \frac{\lambda^2}{z - \mu e^{-i\psi}} \tag{1}$$

maps that circle into a Joukowski aerofoil in the ζ $(= \xi + i\eta)$-plane shown in Fig. 1. In equation (1) λ, μ and ψ are constants with $\lambda = -\mu\cos\psi + (1 - \mu^2\sin^2\psi)^{1/2}$, $0 \leqslant \psi \leqslant \frac{1}{2}\pi$. We note that μ provides a measure of the thickness of the aerofoil, ψ a measure of its camber and the point $z = \mu e^{-i\psi} + \lambda$ is a singular point of the mapping that corresponds to the sharp trailing edge of the aerofoil.

Consider next a uniform flow, speed U_0, past the circular cylinder, inclined at angle α to the x axis, and suppose that there is circulation K about the cylinder. The circulation is chosen such that $z = \mu e^{-i\psi} + \lambda = e^{-i\beta}$ is a stagnation point. This corresponds to smooth flow from the trailing edge of the aerofoil, and results

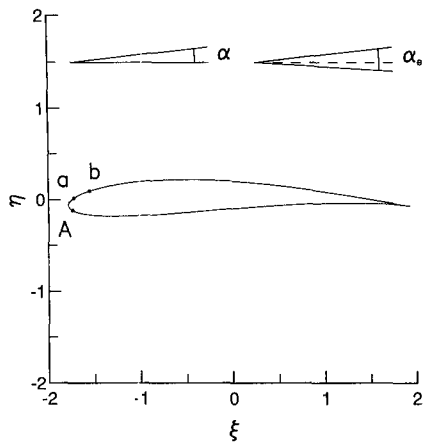

Fig. 1. Definition sketch. A Joukowski aerofoil with $\mu = 0.1$, $\psi = 0.68$. The angles α, α_e are the incidence and effective incidence respectively. A denotes the point of attachment; a, b the ends of the slot.

in $K = -4\pi \sin(\alpha+\beta)$. Since the lift L on the aerofoil is proportional to K we have $L = 0$ when $\alpha = -\beta$, and this leads in turn to the definition of an effective incidence $\alpha_e = \alpha+\beta$.

The complex potential for the flow in the z plane is, in dimensionless form with U_0 as a scale for velocity,

$$w(z) = z\,e^{-i\alpha} + e^{i\alpha}/z + \{e^{i(\alpha+\beta)} - e^{-i(\alpha+\beta)}\}\log z. \quad (2)$$

From this complex potential, and (1), we have the complex velocity in the ζ plane given as

$$\frac{dw}{d\zeta} = \frac{(z-\mu e^{-i\psi})^2\{z+e^{i(2\alpha+\beta)}\}\,e^{-i\alpha}}{z^2(z-\mu e^{-i\psi}+\lambda)}. \quad (3)$$

We see immediately that the stagnation point on the aerofoil is located at the point corresponding to $z = -e^{i(2\alpha+\beta)}$, or $\theta = 2\alpha+\beta+\pi$. For our boundary-layer calculation, described in Section 3 below, it is convenient to take this stagnation point as the origin. With ϕ measured from this point we have $\phi = 2\alpha+\beta+\pi-\theta$. The slip velocity at the surface of the aerofoil, which provides the outer boundary condition for our boundary-layer calculation, is obtained from $|dw/d\zeta|_{z=e^{i\theta}}$ which, when expressed in terms of the new co-ordinate ϕ, gives

$$u_e(\phi) = 2\sin\tfrac{1}{2}\phi \left[\frac{2+2\cos(2\alpha+2\beta-\phi)+\lambda^2 - 2\lambda\{\cos(2\alpha+\beta-\phi)+\cos\beta\}}{2+2\cos(2\alpha+2\beta-\phi)+4\lambda^2 - 4\lambda\{\cos(2\alpha+\beta-\phi)+\cos\beta\}}\right]^{1/2}. \quad (4)$$

From Bernoulli's equation the surface pressure, made dimensionless with $\frac{1}{2}\rho U_0^2$, where ρ is the fluid density, is given from

$$p - p_0 = 1 - u_e^2 \quad (5)$$

where p_0 is the dimensionless free-stream pressure.

2.2. *The perturbed inviscid flow*

The inviscid flow outside the boundary layer, discussed above, will be modified by both the injected fluid and the boundary-layer displacement effect. These are discussed in the next section. Both effects are assumed to be small, and can be represented as sources distributed over the surface of the aerofoil. From the source distribution it is possible to estimate the increment in the inviscid slip velocity at the surface. It is convenient, for our purposes, to evaluate this in the z plane. Denoting the increment by Δu_e we have

$$\Delta u_e = -\frac{\varepsilon}{2\pi}\int_0^{2\pi} \frac{S_0 \sin(t-\phi)}{1-\cos(t-\phi)}\,dt \quad (6)$$

where S_0 represents the distributed source and ε is a measure of its strength to which we return below. Our hierarchical approach to the problem under consideration assumes that $\Delta u_e \ll 1$.

3. THE VISCOUS BOUNDARY LAYER

We define a Reynolds number, based on the aerofoil chord c, as $Re = U_0 c/\nu$ where ν is the kinematic viscosity of the fluid. We work with boundary-layer co-ordinates (s, y), where s is arc-length measured along the aerofoil surface and y is a scaled co-ordinate normal to it, such that if n is a normal co-ordinate then $y = Re^{-1/2}n$. The corresponding velocity components are (u, v) where the normal component also results from scaling with $Re^{-1/2}$. With this co-ordinate system the dimensionless boundary-layer equations may be written as,

$$\left.\begin{aligned} \frac{\partial u}{\partial s} + \frac{\partial v}{\partial y} &= 0 \\ u\frac{\partial u}{\partial s} + v\frac{\partial u}{\partial y} &= u_e\frac{du_e}{ds} + \frac{\partial^2 u}{\partial y^2} \end{aligned}\right\} \quad (7a,b)$$

where u_e is given by (4), in terms of the angle ϕ. The relationship between s and ϕ is

$$s = \int_0^{\phi}\left[\left(\frac{d\xi}{d\phi}\right)^2 + \left(\frac{d\eta}{d\phi}\right)^2\right]^{1/2} d\phi \quad (8)$$

where (ξ, η) are the real and imaginary parts respectively of ζ in equation (1), and the integrand of (8) is evaluated at the circular cylinder $z = e^{i\theta}$ in the z plane. When discretizing (7), for computational purposes, we have not used uniform step lengths δs, rather we have taken equal increments $\delta\phi$ in ϕ, from which δs follows according to (8). The advantages of this are first that it proves a convenient way of increasing the density of grid points in the regions of rapid change and second, equal intervals of ϕ are more convenient for evaluating the integral in (6), treated as a Cauchy principal value integral.

The boundary conditions for (7) require that

$$\left.\begin{aligned} u &\to u_e \quad \text{as} \quad y \to \infty, s > 0 \\ u &\equiv 0 \quad \text{at} \quad s = 0, y \geqslant 0 \end{aligned}\right\} \tag{9a,b}$$

together with conditions at $y = 0$. These latter conditions must include a simulation of the injected fluid, from a slot, into the boundary layer. If we define

$$u_J = \tfrac{1}{2}\{1 - \tanh[(|s - s_0| - l)/\delta]\} \tag{10}$$

then we write, at $y = 0$, $s > 0$

$$\left.\begin{aligned} u &= Ju_J \cos\chi \\ v &= Ju_J \sin\chi. \end{aligned}\right\} \tag{11a,b}$$

Equations (10) and (11) represent a jet issuing from a slot, at angle $\chi = \tan^{-1}(v/u)$ to the boundary; note that this is small on account of the boundary-layer scaling on v. In (10), (11), s_0 represents the centre of the slot, l is a measure of its length, and δ, assumed small, is a measure of the thickness of the boundary layers which flank what is essentially a 'top hat' profile, the constant J is a measure of the strength of injection from the slot.

Since a consequence of our high-Reynolds number assumption is that the pressure is constant across the boundary layer, the reservoir pressure, p_r, required to maintain (11) is given by $p_r - p_0 = 1 + J^2 - u_{es_0}^2$, where u_{es_0} is the free-stream speed at the slot location s_0.

As we have remarked in Section 2, the displacement effect, due to the injected fluid and viscous effects, will modify the outer inviscid flow according to equation (6), and this we now estimate. From equation (7) we have

$$v + y\frac{\mathrm{d}u_e}{\mathrm{d}s} = v_w + \frac{\partial}{\partial s}\int_0^y (u_e - u)\,\mathrm{d}y. \tag{12}$$

In (12) v_w is the normal velocity at the boundary, defined by (11b). In the absence of viscosity and injection the right-hand side of (12) vanishes and so may be identified as the displacement effect. Evaluating at $y = \infty$ gives, as the required displacement velocity

$$v_d = v_w + \frac{\mathrm{d}}{\mathrm{d}s}\int_0^\infty (u_e - u)\,\mathrm{d}y \tag{13}$$

and so we complete (6) by setting $\varepsilon = Re^{-1/2}$, $S_0 = \bar{v}_d$, where $\bar{v}_d$ is the corresponding displacement velocity in the z plane.

4. THE THERMAL BOUNDARY LAYER

We assume that temperature differences are not sufficiently large as to significantly affect the physical properties of the fluid such as density, viscosity and thermal conductivity. In that case equations (7) are supplemented by

$$u\frac{\partial T}{\partial s} + v\frac{\partial T}{\partial y} = \frac{1}{\sigma}\frac{\partial^2 T}{\partial y^2} \tag{14}$$

where $\sigma = \nu/\kappa$ is the Prandtl number, with κ the thermal diffusivity, and the dimensionless temperature T is defined by

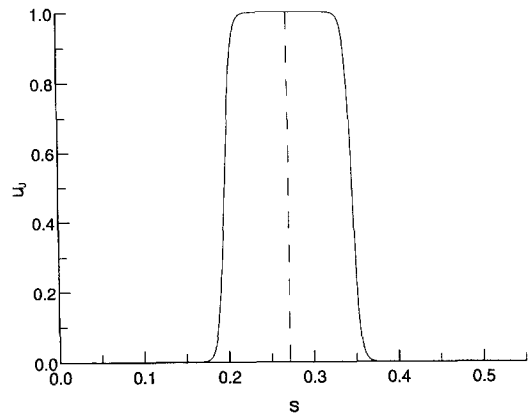

Fig. 2. The injection profile u_J of equation (10) with $s_0 = 0.272$, $l = 0.075$ and $\delta^{-1} = 128$. Arc length is measured from A.

$$T' = T_\infty + (T_w - T_\infty)T \tag{15}$$

where T' is the dimensional temperature, T_∞ the ambient temperature, and T_w a measure of the boundary temperature. Clearly we require

$$T \to 0 \quad \text{as} \quad y \to \infty, \quad s > 0. \tag{16}$$

The temperature distribution at $s = 0$ has to be constructed in the manner described in the next section. There remains the condition to be imposed at $y = 0$.

We envisage two situations. Common features of these are that ahead of the injection slot the wall temperature is a constant, T_w, so that $T = 1$ at $y = 0$, and the injected fluid has a lower temperature. The two cases differ in that beyond the slot we have either (i) the boundary temperature is again maintained at a constant value with $T = 1$ at $y = 0$ or (ii) the boundary is thermally insulated with $\partial T/\partial y = 0$ at $y = 0$. In case (i) a measure of the cooling effect is the amount of heat added that is necessary to maintain the boundary temperature and in case (ii) the temperature of the boundary itself is measured. For case (i) we take, at $y = 0$

$$T = T_0[1 - \tanh\{(|s - s_0| - l)/\delta\}] + 1 \tag{17}$$

whilst for case (ii) we take

$$\left.\begin{aligned} T &= T_0[1 - \tanh\{(s_0 - s - l)/\delta\}] + 1 \quad s \leqslant s_J \\ \partial T/\partial y &= S(s)\,\partial T/\partial y|_{s=s_J} \quad s_J \leqslant s \leqslant s_b \\ \partial T/\partial y &= 0 \quad s > s_b. \end{aligned}\right\} \tag{18}$$

In (18) s_b is the notional end of the slot, defined as the point at which $u_J = 0.01$ and s_J the point at which $u_J = 0.9$ immediately upstream, see Fig. 2. $S(s)$ is a suitably chosen smoothing function with $0 \leqslant S \leqslant 1$.

5. NUMERICAL PROCEDURES

In this section we outline the numerical procedures we have employed to obtain the solutions that are described in Section 6 below. We begin with the non-linear system (7), together with the boundary conditions (9) and (11). First it is necessary to consider the nature of the solution close to $s = 0$. From (4) and (8) we find, after some manipulation, that for $s \ll 1$

$$u_e = Bs + O(s^2) \tag{19}$$

where

$$\left.\begin{aligned} B = h^2\{h + 3\lambda^2 - 2\lambda[\cos(2\alpha+\beta) + \cos\beta]\}^{-1/2} \\ \times \{6h - 6 + 2\lambda^2[1 + 4\cos 2(\alpha+\beta)] \\ + 2\cos 4(\alpha+\beta) - 4\cos 2(\alpha+\beta) \\ - 4\lambda[\cos(2\alpha+3\beta) + \cos(4\alpha+3\beta)]\}^{-1/2} \end{aligned}\right\} \tag{20}$$

with

$$h = 2 + 2\cos 2(\alpha+\beta) + \lambda^2 - 2\lambda[\cos(2\alpha+\beta) + \cos\beta].$$

If we then write

$$u = Bsf(y) + O(s^2) \quad v = Bg(y) + O(s) \tag{21}$$

the equations satisfied by f and g are, from (7),

$$\text{with} \quad \left.\begin{aligned} B^{-1}f'' - gf' - f^2 + 1 = 0 \quad f + g' = 0 \\ f(0) = g(0) = 0 \qquad f(\infty) = 1. \end{aligned}\right\} \tag{22}$$

The method of solution of (22) mirrors what we have used when advancing the solution of (7) step by step, and we do not describe it in detail. Rather, we concentrate on the solution of (7) and the technique for advancing it in the direction of increasing s, in either direction, from the stagnation point $s = 0$. The finite-difference mesh we introduce is uniform in the y direction, with step length δy such that $y_j = j\delta y$, $j = 0, 1, \ldots, n+1$ with the assumed edge of the boundary layer at $y_\infty = (n+1)\delta y$. In the s direction, as we have already indicated, the step-length is non-uniform such that the mesh is finer in regions where flow quantities change more rapidly than elsewhere. If $\delta s_i = s_{i+1} - s_i$ then we have $s_i = \Sigma_{r=0}^{i-1} \delta s_r$. In advancing the solution from s_i to s_{i+1}, that is from station i to $i+1$ we discretize (7) using central differences. The solution is known at s_i, and it is the $2n$ quantities $u_{i+1,j}$, $v_{i+1,j}$, $j = 1, \ldots, n$ that are to be determined as s_{i+1}. The discretized equations (7) provide $2n$ non-linear equations to solve for these quantities where, in these equations, use of the conditions (9) and (11) has been made to eliminate $u_{i+1,0}$, $v_{i+1,0}$ and $u_{i+1,n+1}$. At each station an initial estimate of the flow quantities is made either by extrapolation from the two previous stations or, at $s = \delta s_0$ ($s_0 = 0$), by use of (21). Since the discretized forms of (7) are non-linear the solution is completed iteratively. So, if $\mathbf{X}$ represents the solution vector with elements $u_{i+1,j}$, $v_{i+1,j}$ and $\mathbf{X}^r$ is the rth estimate of it, and if $\mathbf{F}$ is a vector whose $2n$ components are the discretized form of (7), then $\mathbf{X}$ satisfies

$$\mathbf{O} = \mathbf{F}(\mathbf{X}) \approx \mathbf{F}(\mathbf{X}^r) + \mathbf{Ja} \cdot (\mathbf{X} - \mathbf{X}^r) \tag{23}$$

where $\mathbf{Ja}$ is the Jacobian matrix of the system evaluated at $\mathbf{X}^r$, that is the matrix with elements $\partial F_i/\partial X_j$ in its ith row and jth column. Equation (23) forms the basis of our iterative method with

$$\mathbf{X}^{r+1} = \mathbf{X}^r - \mathbf{Ja}^{-1} \cdot \mathbf{F}(\mathbf{X}^r)$$

or

$$\mathbf{Ja} \cdot \delta\mathbf{X}^r = -\mathbf{F}(\mathbf{X}^r) \tag{24}$$

which is solved iteratively until $|\delta\mathbf{X}^r|$ is less than some prescribed tolerance. The solution procedure for (24) is implemented as follows. The components of $\mathbf{X}$ are defined as

$$\left.\begin{aligned} X_{2j-1} = u_{i+1,j} \\ X_{2j} = v_{i+1,j} \quad j = 1, \ldots, n \end{aligned}\right\} \tag{25}$$

with the corresponding components of $\mathbf{F}$ given from the discretized versions of equations (7b) and (7a), respectively. The Jacobian matrix is then of block tri-diagonal form with elements that are themselves 2×2 matrices. The matrix $\mathbf{Ja}$ is then decomposed as $\mathbf{Ja} = \mathbf{L}\,\mathbf{U}$ where $\mathbf{L}$ is a lower unitary block bi-diagonal matrix, and $\mathbf{U}$ is an upper block bi-diagonal matrix. The elements of both $\mathbf{L}$ and $\mathbf{U}$ are again 2×2 matrices. The advantages of this decomposition lie in the more efficient solution procedure for (24) as follows. First define

$$\left.\begin{aligned} \mathbf{Y} = \mathbf{L}^{-1}\mathbf{F}(\mathbf{X}^r) \\ \text{so that } \delta\mathbf{X}^r \text{ is obtained from} \\ \mathbf{U}\delta\mathbf{X}^r = -\mathbf{Y}. \end{aligned}\right\} \tag{26}$$

This two-step approach to the iterative solution of (24) proves efficient and reliable in practice.

The step-by-step solution of (7), as described above, continues until the trailing edge of the aerofoil is reached (the solution, in fact, never goes beyond the penultimate station since, although the velocity at the trailing edge of a Joukowski aerofoil is non-zero and finite, the pressure gradient is infinite) or the flow separates. Separation is characterized by the vanishing of the shear stress $\tau = \partial u/\partial y|_{y=0}$. If s_p is the separation point then it is known that τ varies as $(s_p - s)^{1/2}$ as that point is approached. The solution method fails in response to this singular behaviour. If s_m, s_{m-1} are the last two stations at which a converged solution is obtained, then s_p is estimated from

$$s_p = s_m + \frac{(s_m - s_{m-1})\tau_m^2}{\tau_{m-1}^2 - \tau_m^2}. \tag{27}$$

With the velocity field determined, the solution of (14) for T is straightforward. For the solution at the initial line $s = 0$ we write

$$T = T_1(y) + O(s) \tag{28}$$

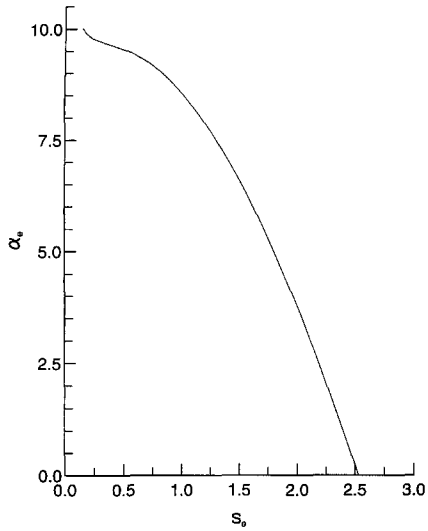

Fig. 3. The position of separation as a function of effective incidence α_e. Here arc length s_e is measured from the point of attachment at $\alpha_e = 0$.

so that with u, v given from (21) the equation for T_1 is

$$Bg\frac{\partial T_1}{\partial y} = \frac{1}{\sigma}\frac{\partial^2 T_1}{\partial y^2} \tag{29}$$

which is to be solved subject to $T_1(0) = 1$, $T_1(\infty) = 0$. Again, the method of solution mirrors that for the step-by-step solution which we now describe. With the same mesh as for the velocity field, and with (14) discretized using central differences, our task is to find the values of $T_{i+1,j}$, $j = 1,\ldots,n$. The discretized equation leads to the following set of algebraic equations

$$a_j T_{i+1,j+1} + b_j T_{i+1,j} + c_j T_{i+1,j-1} = d_j \quad j = 1,\ldots,n \tag{30}$$

where the coefficients a_j, b_j, c_j, and the quantities d_j are all known. When the boundary conditions (16) and (17) or (18) are used $T_{i+1,n+1}$ and $T_{i+1,0}$ in (30) are determined which leaves n equations to be solved for the n unknowns $T_{i+1,j}$, $j = 1,\ldots,n$. The matrix of coefficients in (30) is of tri-diagonal form, and the solution is easily obtained.

6. RESULTS

The aerofoil on which our calculations are based is a cambered, 10% thick aerofoil which corresponds to $\mu = 0.1$, $\psi = 0.68$ in equation (1). This aerofoil is shown in Fig. 1; for it the effective angle of incidence is $\alpha_e = \alpha + 3.6°$.

We first calculate the boundary layer on the upper surface of the aerofoil from equations (7), with u_e given from (4) and (8) and estimate the position of the separation point, from the numerical solution, using equation (27). The separation point so calculated is shown in Fig. 3, for values of α_e increasing from zero, as a function of arc length along the surface measured from the attachment point at $\alpha_e = 0$. The position of the attachment point itself, of course, varies slightly with incidence. Separation at no lift is just beyond mid-chord and, as may be expected, moves rapidly forward as incidence increases until for $\alpha_e = 10°$ the flow remains attached for only a short distance on the upper surface.

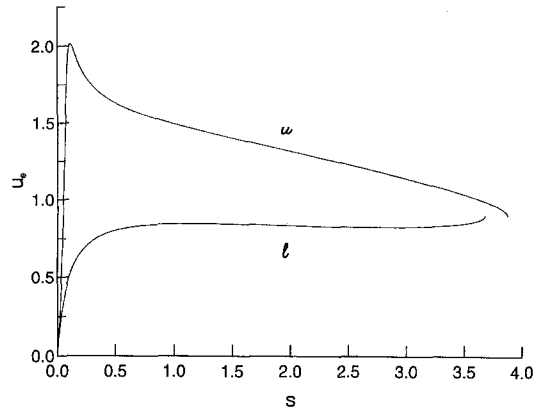

Fig. 4. The inviscid slip velocity u_e on the upper (u) and lower (l) surfaces of the aerofoil shown in Fig. 1 for $\alpha = 6.3°$. Arc length is measured from A.

To investigate the effect of slot injection on separation we take the relatively high incidence of $\alpha = 6.3°$, which corresponds to an effective incidence $\alpha_e = 9.9°$. The inviscid slip velocities on both the upper and lower surfaces, with corresponding pressure distributions, are shown in Figs. 4 and 5 respectively. We remark that the arc length from attachment, denoted by A in Fig. 1, to the trailing edge of the aerofoil is greater on the upper than the lower surface. We see that on the upper surface of the aerofoil an initial favourable pressure gradient rapidly gives way to a severe adverse gradient which the boundary layer is unable to sustain, with separation taking place at $s = 0.285$. To counter this adverse gradient we centre our injection slot at $s = 0.272$. Thus, in the definition

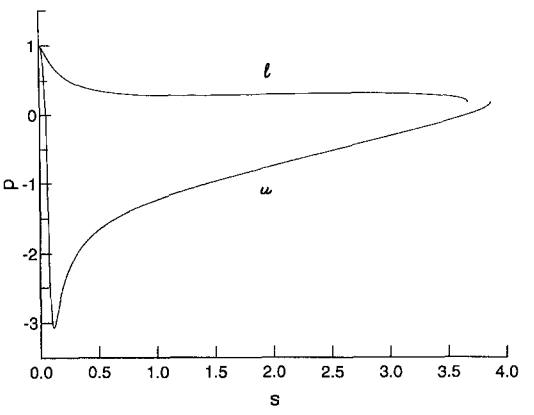

Fig. 5. The pressure distribution p on the upper (u) and lower (l) surfaces of the aerofoil shown in Fig. 1 for $\alpha = 6.3°$. Arc length is measured from A.

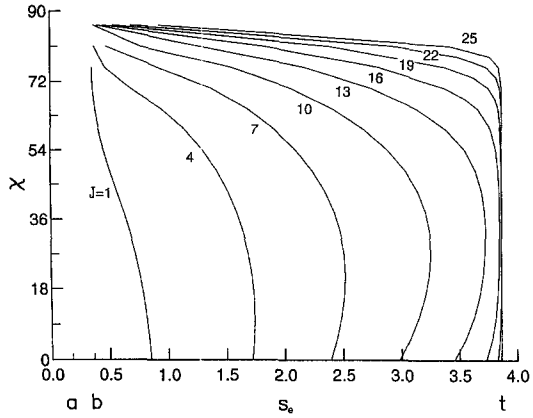

Fig. 6. Variation of the position of separation s_e with the injection angle χ, for various values of J. Arc length is measured from the point of attachment A. The edges of the slot are at $s_e = 0.18$ denoted as a, $s_e = 0.36$ denoted as b. Separation occurs at $s_e = 0.285$ when $J = 0$. The upper surface of the aerofoil measures 3.869 units of arc length, and the trailing edge is shown as t.

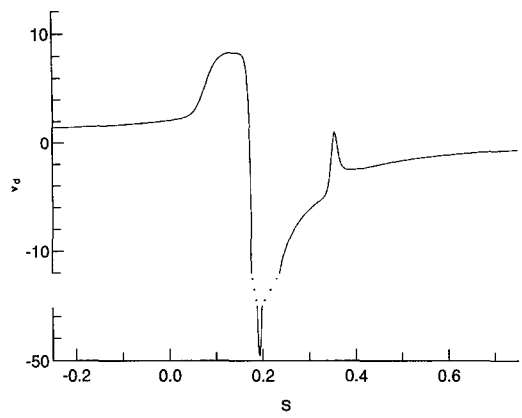

Fig. 7. The viscous displacement velocity in the neighbourhood of the injection slot for the case $J = 20$, $\chi = 36°$.

of u_J in equation (10), we take $s_0 = 0.272$, $l = 0.075$, $\delta^{-1} = 128$. This essentially 'top-hat' injection profile is shown in Fig. 2. We define the edges of our simulated slot to be the points at which $u_J = 0.01$, so that in this particular case the slot is in the region $0.18 \leqslant s \leqslant 0.36$. The edges of the slot are indicated in Fig. 1.

To assess the effects of injection we note from (11) that two parameters are available to us, namely the magnitude, or strength, of the injection J, and the angle χ at which the injected fluid initially penetrates the boundary layer. Note that although we may vary χ by an O(1) amount, the boundary-layer scaling that is implicit in the definition of χ means that in all cases we are injecting fluid close to the boundary. In Fig. 6 we show the effect of slot-blowing on the separation position. For a fixed value of χ we see, as perhaps expected, that separation is delayed as J increases. Somewhat unexpected is that for a given value of $J \gtrsim 4$ the separation position does not vary monotonically with χ. For $J \gtrsim 10$ the optimum injection angle is approximately 36°. At that angle, when $J \gtrsim 18$, separation is postponed to the trailing edge. The boundary layer on the lower surface is unaffected by injection into the boundary layer on the upper surface, and remains attached at this incidence. As a consequence we find that by blowing sufficiently hard it is possible to maintain a wholly attached flow at this incidence. Whilst the injection strength J may appear to be large for this to be so, the mass injection to achieve this is relatively modest, $O(Re^{-1/2}J)$, for high Reynolds numbers.

As we have already indicated in Section 2, the displacement effect associated with injection and viscosity may lead to a significant modification of the outer, inviscid, flow. For the case $J = 20$, $\chi = 36°$, we show in Fig. 7 the displacement velocity defined by equation (13). In all of the above calculations the edge of the boundary layer, $y = \infty$, was represented by $y_\infty = 10.0$, and 1001 points were used to resolve the boundary layer, corresponding to an increment $\delta y = 10^{-2}$. With the displacement velocity given, we may calculate the change in the inviscid slip velocity at the surface that this brings about. To do this we revert to the z plane, and equation (6). The integrand in this equation is tabulated at 1600 equally spaced points such that $\delta\phi = \pi/800$. Such fine resolution enables us to evaluate the Cauchy principal value integral in (6) quite accurately using the trapezium rule. In the ζ plane the corresponding tabular points are not equally spaced in s. On both the upper and lower surfaces of the aerofoil we have, in the mid-section $\delta s \approx 7 \times 10^{-3}$, whilst in the nose region $\delta s \approx 1.05 \times 10^{-3}$. High resolution close to the leading edge ensures that all flow properties are well resolved. Returning to (6) we show in Fig. 8 the quantity $Re^{1/2}\Delta u_e$ we have calculated, where Δu_e is the increment in the slip velocity on the aerofoil, as a function of arc length. This quantity peaks sharply just ahead of the slot, which may be expected as the flow anticipates the injection of fluid. We see from Fig. 8 that higher-order effects will be unimportant for $Re \gtrsim 10^4$.

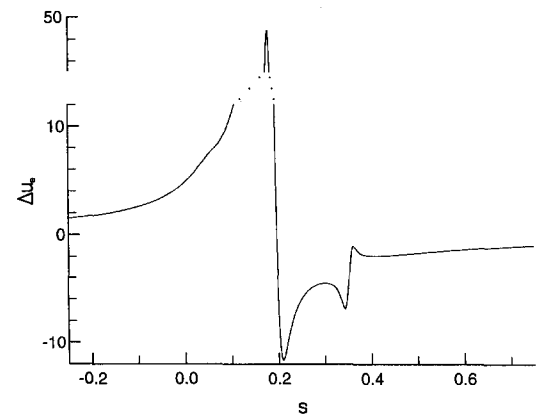

Fig. 8. The increment of inviscid slip velocity which corresponds to the displacement velocity of Fig. 7.

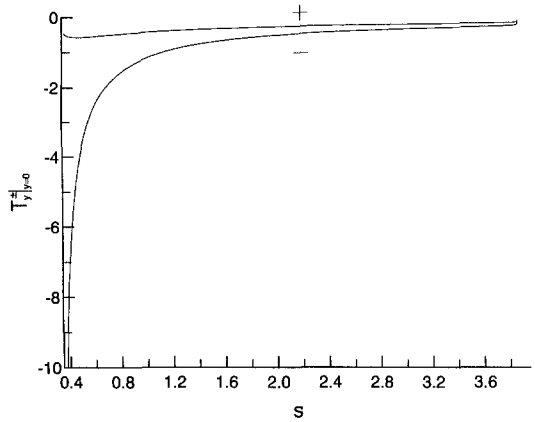

Fig. 9. The heat transfer parameter, $\partial T/\partial y|_{y=0}$, downstream from the slot, for slot temperature $T = 1$, '+', and for slot temperature $T = -1$, '−'.

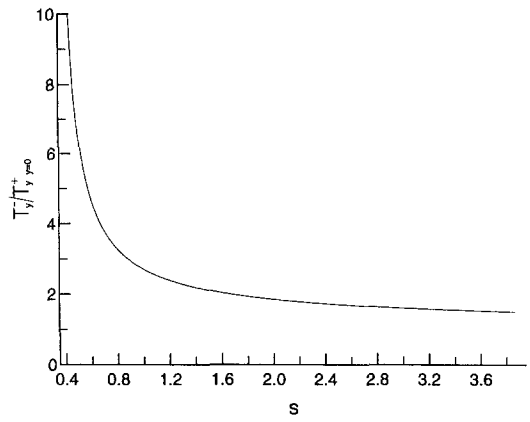

Fig. 10. The ratio of the heat transfer parameters shown in Fig. 9.

We next consider the heat transfer characteristics associated with injection when the injected fluid has a temperature different from both the ambient temperature, and the constant boundary temperature T_w ahead of the slot. For comparison purposes we also consider the case when the injected fluid has temperature T_w. The two situations we consider are outlined in Section 4. In case (i), to which (17) refers, the boundary temperature reverts to its value ahead of the slot, whilst in case (ii) we have an adiabatic wall condition as in equation (18). We set the Prandtl number $\sigma = 0.7$ and maintain the blowing strength as $J = 20$, so that the boundary layer remains attached.

We consider, first, case (i) for which the boundary condition (17) is appropriate. In (17) we take $T_0 \equiv 0$ initially so that the injected fluid has the same temperature, $T = 1$, as the boundary temperature. In that case a layer of fluid at wall temperature is introduced over the surface of the aerofoil. As a consequence the heat transfer from the surface, proportional to $-\partial T/\partial y$, is relatively small, as is shown in Fig. 9. We next take $T_0 = -1$ in (17) in which case the injected fluid has temperature $T = -1$, much cooler than the ambient or wall temperatures. Now a layer of cold fluid is introduced over the surface downstream from the slot. The effect of this is a much larger heat transfer to the fluid, from the aerofoil surface. This is also shown in Fig. 9. We may interpret the heat transfer in this case as a measure of the heat that must be supplied to maintain a uniform surface temperature or, alternatively, as a measure of the cooling effect associated with the injection of cooler fluid. This is emphasized in Fig. 10 where, from the results shown in Fig. 9, we demonstrate the effectiveness of injecting cold fluid by making a direct comparison with the case when the injected fluid is at the boundary temperature.

We next consider case (ii) with the boundary conditions (18). In (18) we have taken the smoothing function as $S(s) = \exp[-200(s-s_J)]$. As with case (i) we carry out calculations with both $T_0 = 0$ and $T_0 = -1$. In the first of these the temperature of the injected fluid, $T = 1$, is again that of the boundary temperature ahead of the slot, whilst for the second the injected fluid is cooled to $T = -1$. We denote the subsequent temperature distributions for $s > s_b$ by $T^+(y)$ and $T^-(y)$ respectively. An important feature to note is the following. At the injection rate $J = 20$ that we have adopted, the temperature distribution at $s = s_b$ is almost independent of conditions ahead of the slot so that $T^+(y) \approx -T^-(y)$ at $s = s_b$. This is demonstrated in Fig. 11. In this case, with the same homogeneous boundary conditions downstream from the slot, it follows that $T^+(y) \approx -T^-(y)$ for all $s > s_b$. For the adiabatic wall condition, when $s > s_b$, a direct measure of the boundary cooling is the temperature of the boundary itself, $T(0)$. We show in Fig. 12 the distributions $T^+(0)$ and $T^-(0)$, and we note the substantial cooling of the boundary in the latter case. We see from Fig. 12 that indeed $T^+(0) \approx -T^-(0)$ and this is further emphasized in Fig. 13 where these quantities are compared directly. On this evidence we may infer the useful result that the boundary temperature in $s > s_b$ may be calculated, to a good approximation, from T^+ as $(2T_0+1)T^+(0)$.

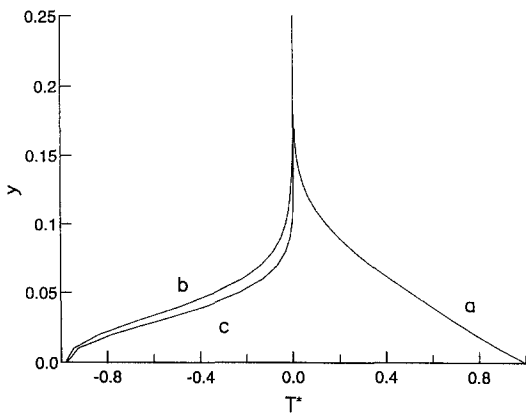

Fig. 11. Temperature distributions at the commencement of the slot $s = s_a$, (a) where $T^+(y) = T^-(y)$, and at the end $s = s_b$ where $-T^+(y)$ is denoted by (b), $T^-(y)$ by (c).

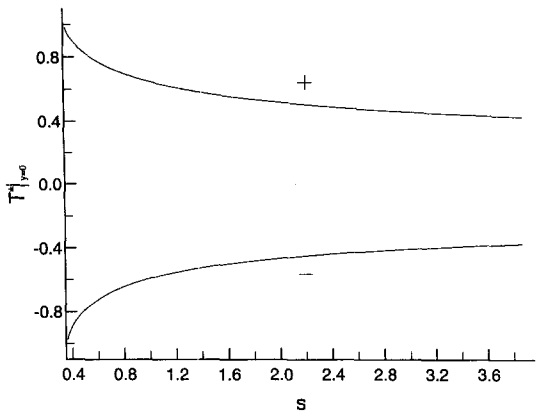

Fig. 12. The wall temperature, $T^{\pm}|_{y=0}$ downstream from the slot, for slot temperature $T = 1$, '+', and for slot temperature $T = -1$, '−'.

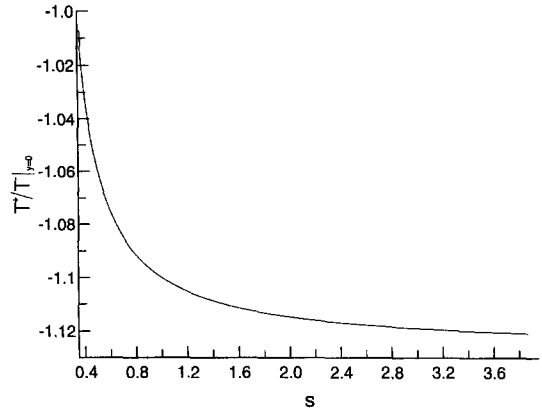

Fig. 13. The ratio of the wall temperatures shown in Fig. 12.

7. CONCLUSIONS

In this paper we have demonstrated that laminar flow separation on an aerofoil, which at sufficiently high incidence will be close to the leading edge, may be delayed to the trailing edge if fluid is injected from a slot close to the leading edge. For this to be achieved the blowing velocity has to be sufficiently high, although the mass injection rate is only modest. If the injected fluid is cooled, then we have shown that a significant cooling of the aerofoil itself is achieved.

Acknowledgements—This work was carried out, in part, under a research agreement between the University of East Anglia and the Department of Trade and Industry, monitored by the Aerodynamics and Propulsion Department of the Defence Research Agency's Aerospace Division at Bedford.

REFERENCES

1. A. D. Fitt, J. R. Ockendon and T. V. Jones, Aerodynamics of slot-film cooling: theory and experiment, *J. Fluid Mech.* **160,** 15–27 (1985).
2. A. D. Fitt and P. Wilmott, Slot film cooling—the effect of separation angle, *Acta Mech.* **103,** 79–88 (1994).
3. J. B. Klemp and A. Acrivos, High Reynolds number flow past a flat plate with strong blowing, *J. Fluid Mech.* **51,** 337–356 (1972).
4. D. Catherall, K. Stewartson and P. G. Williams, Viscous flow past a flat plate with uniform injection, *Proc. R. Soc.* A **284,** 370–396 (1965).
5. F. T. Smith and K. Stewartson, On slot injection into a supersonic laminar boundary layer, *Proc. R. Soc.* A **332,** 1–22 (1973).
6. F. T. Smith and K. Stewartson, Plate-injection into a separated supersonic boundary layer, *J. Fluid Mech.* **58,** 143–159 (1973).
7. N. Riley, Oblique slot blowing into a supersonic laminar boundary layer, *Math. Proc. Camb. Phil. Soc.* **80,** 541–554 (1976).
8. N. Riley, Non-uniform slot injection into a laminar boundary layer, *J. Engng Math.* **15,** 299–314 (1981).
9. R. J. Goldstein, Film cooling, *Adv. Heat Transfer* **7,** 321–379 (1971).